Mechanisms of hopping conductivity in weakly doped $La_{1-x}Ba_xMnO_3$

2005 J. Phys.: Condens. Matter 17 3429

(http://iopscience.iop.org/0953-8984/17/21/033)

INSTITUTE OF PHYSICS PUBLISHING JOURNAL OF PHYSICS: CONDENSED MATTER

J. Phys.: Condens. Matter **17** (2005) 3429–3444 doi:10.1088/0953-8984/17/21/033

Mechanisms of hopping conductivity in weakly doped $La_{1-x}Ba_xMnO_3$

R Laiho[1], K G Lisunov[1,2], E Lähderanta[1,3], M A Shakhov[1,4], V N Stamov[1,2], V S Zakhvalinskii[1,5], V L Kozhevnikov[6], I A Leonidov[6], E B Mitberg[6] and M V Patrakeev[6]

[1] Wihuri Physical Laboratory, University of Turku, FIN-20014 Turku, Finland
[2] Institute of Applied Physics, Academiei Street 5, MD-2028 Kishinev, Moldova
[3] Department of Physics, Lappeenranta University of Technology, PO Box 20, FIN-53851 Lappeenranta, Finland
[4] A F Ioffe Physico-Technical Institute, 194021 St Petersburg, Russia
[5] Belgorod State University, Pobeda Street 85, 308015 Belgorod, Russia
[6] Institute of Solid State Chemistry, GSP 14591 Pervomaiskaia, 620219 Ekaterinburg, Russia

Received 23 February 2005, in final form 11 April 2005
Published 13 May 2005
Online at stacks.iop.org/JPhysCM/17/3429

Abstract

The resistivity, ρ, of ceramic $La_{1-x}Ba_xMnO_3$ with $x = 0.02$–0.10 corresponding to the concentrations of holes $c \approx 0.15$–0.17 displays an activated behaviour both above and below the paramagnetic to ferromagnetic transition temperature $T_C = 175$–209 K, obtained from measurements of the magnetization. Above $T \sim 310$–390 K $\rho(T, x)$ is determined by nearest-neighbour hopping of small polarons with activation energy $E_a = 0.20$–0.22 eV. Below the onset temperature $T_v = 250$–280 K, depending on x, a Shklovskii–Efros-like variable-range hopping conductivity mechanism, governed by a soft temperature independent Coulomb gap, $\Delta \approx 0.44$–0.46 eV, and a rigid gap, $\delta(T)$, is found. For the range $T \sim 50$–120 K, $\delta(T)$ is connected to the formation of small lattice polarons in conditions of strong electron–phonon interaction and lattice disorder. The rigid gap obeys a law $\delta(T) \sim T^{1/2}$ within two temperature intervals above and below T_C, exhibits an inflection at T_C and reaches at T_v a value of $\delta_v \approx 0.14$–0.18 eV. Such behaviour suggests a spin dependent contribution to $\delta(T)$. The localization radius of the charge carriers, a, has different constant values within the temperature intervals where $\delta(T) \sim T^{1/2}$. With further decrease of T, a increases according to the law expected for small lattice polarons.

(Some figures in this article are in colour only in the electronic version)

1. Introduction

$La_{1-x}Ba_xMnO_3$ (LBMO) is a hole doped mixed valence manganite perovskite compound exhibiting colossal magnetoresistance (CMR) near the paramagnetic (PM) to ferromagnetic

(FM) transition temperature, T_C [1, 2]. The hole doping by substitution of a divalent alkaline element for La^{3+} or by formation of cation vacancies induces mixed valence $Mn^{3+,4+}$ ions and pairs of Mn^{3+}–Mn^{4+} coupled with FM double-exchange (DE) interaction. Due to competition with Mn^{3+}–Mn^{3+} pairs coupled with the superexchange (SE) interaction, different kinds of spin orderings are realized in different intervals of the temperature, T, the magnetic field, B, and the relative hole concentration c equal to the Mn^{4+}/Mn^{3+} ratio [2, 3]. This leads in conditions of lattice disorder to frustration of the magnetic ground state [4] and appearance of a spin-glass phase [5, 6], or due to phase separation [7, 8] to cluster-glass formation [6, 9].

Electronic properties of weakly doped ($c < 0.15$–0.20) manganite perovskites are governed by electron localization, presumably due to strong electron–phonon interaction and the local Jahn–Teller distortions [10], leading to the formation of a small polaron state [11]. The resistivity, $\rho(T)$, displays an activated (or semiconductor-like) behaviour, decreasing exponentially with T ($d\rho/dT < 0$) both above and below T_C, and having an inflection around T_C [12]. At higher doping levels delocalization of the electrons near T_C leads to a metal–insulator transition (MIT), which corresponds to transformation of $\rho(T)$ from the activated behaviour at $T > T_C$ to the metallic ($d\rho/dT > 0$) behaviour at $T < T_C$ [2, 12]. Nearest-neighbour hopping (NNH) conductivity of small polarons satisfying the Arrhenius law is observed above the room temperature in various perovskite materials [2, 12], persisting in $La_{1-x}Ca_xMnO_3$ up to $T \sim 700$ K [13] and 1200 K [14]. However, on lowering the temperature deviations from the NNH conductivity are observed, suggesting a transition to variable-range hopping (VRH) conductivity [15] similar to that in disordered systems like doped semiconductors [16], where the hopping conductivity is strongly influenced by details of the one-electron density $g(\varepsilon)$ of the localized states (DOS) near the Fermi level, μ [16].

In manganite perovskites the structure of DOS is complex around μ, including a parabolic interval with width $\Delta \sim 0.5$ eV (soft gap) and a region of $g(\varepsilon) = 0$ with width $\delta(T)$ up to ~0.11 eV (rigid gap), as determined by scanning tunnelling spectroscopy of a $La_{0.8}Ca_{0.2}MnO_3$ film [17]. The soft or the Coulomb [16] gap is attributed to Coulomb interactions between localized charge carriers, and is much wider in the manganites than in the doped semiconductors having $\Delta \sim 1$–10 meV [18]. This can be explained by the much higher (by ~4–6 orders of the magnitude) concentrations of charge carriers in the manganites, enhancing considerably the Coulomb correlation effects. On the other hand, the rigid gap $\delta(T)$ can be ascribed in the perovskite oxide compounds to polaron formation. Indeed, to hop from a site below μ to another site above μ the carrier should annihilate the polarization on the initial site and create it on the final site. This requires a minimum hopping energy, which may lead to a rigid gap around μ, if the polarization of the surrounding ions is the main reason for the localization of the charge carriers, whereas that from the lattice disorder is much smaller. This situation is expected to be realized in the manganite perovskites.

Although the Coulomb correlations and formation of small polaron states are multi-electron effects, the analysis of the VRH conductivity in the manganites using the one-electron DOS containing the gaps Δ and δ yields reasonable results. The localization radii of the charge carriers, $a \approx 2.5$–2.9 Å in $La_{0.7}Ca_{0.3}Mn_{1-y}Fe_yO_3$ [15] and 1.2–1.7 Å in $LaMnO_{3+\eta}$ [19], satisfy the condition of small polaron radius [20]. The values of $\Delta \approx 0.40$–0.44 eV for $La_{0.7}Ca_{0.3}Mn_{1-y}Fe_yO_3$ [15] and 0.43–0.48 eV in $LaMnO_{3+\eta}$ [19] are similar to the Coulomb interaction energy at an average distance between the carriers and close to the experimental values of Δ obtained by scanning tunnelling spectroscopy in $La_{0.8}Ca_{0.2}MnO_3$ [17]. In addition, at T well above T_C the rigid gap follows for both compounds the law $\delta(T) \approx \delta_v(T/T_v)^{1/2}$, where T_v is the onset temperature of the VRH conductivity, $\delta_v \approx 0.16$–0.12 eV for $La_{0.7}Ca_{0.3}Mn_{1-y}Fe_yO_3$, decreasing with y [15] and $\delta_v \approx 0.14$–0.17 eV for $LaMnO_{3+\eta}$, increasing with η [19]. The values of δ_v are similar to those found in [17] and the dependences

of δ_v on y and η are consistent with increasing lattice disorder in $La_{0.7}Ca_{0.3}Mn_{1-y}Fe_yO_3$ when y is increased [15] and with progressive lattice distortions in $LaMnO_{3+\eta}$ when η is increased [19]. The properties of Δ and $\delta(T)$ have been utilized for quantitative interpretation of the thermopower in $La_{0.7}Ca_{0.3}Mn_{1-y}Fe_yO_3$ under a magnetic field [21].

Up to now the manganite perovskites doped with Ca or Sr have been investigated most extensively [2, 12]. LBMO demonstrates a series of electronic and magnetic properties as well as CMR typical of Ca or Sr doped manganites [22–24], stimulating general interest in this compound. In the present paper we investigate the resistivity of weakly doped LBMO, expected to exhibit activated conductivity well below the room temperature due to absence of the MIT, as is common in the CMR materials with low doping levels. This allows us to obtain detailed information about the mechanisms of the hopping charge transfer in wide temperature intervals above and below T_C.

2. Experimental results

LBMO samples with $x = 0.02$, 0.04, 0.08 and 0.10 marked below as No 2, No 4, No 8 and No 10, respectively, were synthesized with the conventional solid state reaction method from La_2O_3, Mn_3O_4 and $BaCO_3$. The raw materials were pre-calcined to remove possible adsorbates, weighed in stoichiometric proportions and mixed with addition of ethanol. The mixtures were pressed into pellets and fired at 900–1300 °C in air, crushed into powder and pressed and fired several times with gradually increasing temperature until single-phase material was obtained. The phase purity and the lattice structure were determined with room temperature x-ray powder diffraction investigations ($\lambda = 1.541\,78$ Å), establishing the rhombohedral $R\bar{3}c$ space group. The values of the lattice parameters $a = b = 5.521$–5.535 Å and $c = 13.348$–13.444 Å (increasing with x) agree closely with those in [25].

Investigations of $\rho(T)$ were made for $T = 25$–450 K using the conventional four-probe technique in a transverse magnetic field configuration ($\mathbf{B} \perp \mathbf{j}$) for $B = 0$–10 T, increasing and decreasing the temperature and the magnetic field. Magnetization $M(T)$ was measured with an RF-SQUID magnetometer after cooling the sample from the room temperature down to 5 K in zero dc field (M_{ZFC} or zero-field cooled magnetization) or in a field of $B = 10$ G (M_{FC} or field cooled magnetization).

The plots of the susceptibilities $\chi_{ZFC}(T) = M_{ZFC}(T)/B$ and $\chi_{FC}(T) = M_{FC}(T)/B$ shown in the inset to figure 1 exhibit in all LBMO samples a steep PM–FM transition with T_C increasing with increasing x. The values of T_C are collected in table 1 (for No 8, $T_C = 200$ K). In addition, magnetic irreversibility or deviation of $\chi_{ZFC}(T)$ from $\chi_{FC}(T)$ is observed below the PM–FM transition (an example is shown for No 2), indicating frustration of the magnetic ground state in LBMO to be common in the manganite perovskites with low x [5, 6, 26, 27].

The plots of $\rho(T)$ shown in figure 1 display for all the samples No 2–No 10 an activated behaviour above and below T_C with no signs of the MIT, as can be expected for weakly doped manganites. Near T_C the $\rho(T)$ curve has an inflection, which is more pronounced when x is increased. As can be seen from figure 2, the magnetoresistance of LBMO decreases strongly in the magnetic field, with the maximum variation being near T_C.

3. Theoretical consideration and formulation of the model

For the subsequent analysis of the data we consider electrons, localized by polarization of the medium, $E_p = E_{pL} + E_{pS}$, and by microscopic lattice disorder creating a distribution of the electron potential energy with width $2E_d = 2(E_{dL} + E_{dS})$. Here E_{pL} and E_{pS} are contributions

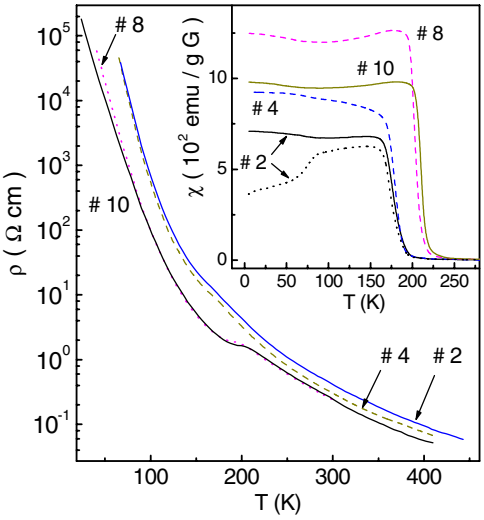

Figure 1. Temperature dependence of the resistivity in zero field. Inset: temperature dependence of χ_{FC} (solid and dashed lines) and χ_{ZFC} (dotted line) in the field $B = 10$ G.

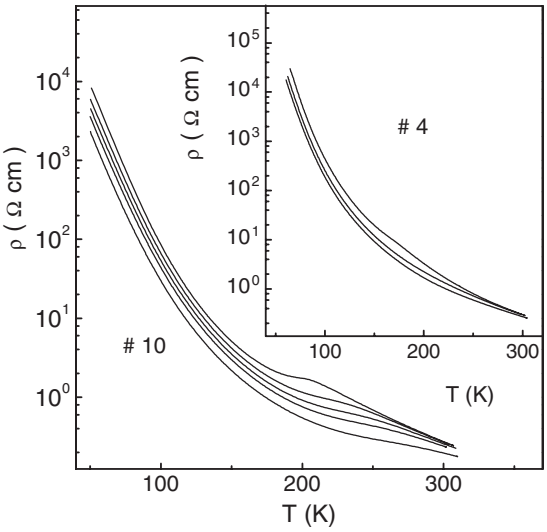

Figure 2. Temperature dependence of the resistivity of No 10 in fields of $B = 0$, 2, 4, 6 and 10 T (from top to bottom). Inset: temperature dependence of the resistivity of No 4 in fields of $B = 0$, 6 and 10 T (from top to bottom).

Table 1. The values the PM–FM transition temperature T_C, the prefactor coefficients of the NNH conductivity A_1 and $A_{3/2}$, the activation energies of the NNH conductivity $E_a^{(1)}$ and $E_a^{(3/2)}$, the transfer integral J, the lower border of the NNH conductivity T_n and the crossover temperature T_{cr}.

Sample Nos	T_C (K)	A_1 (10^{-7} Ω cm K^{-1})	$A_{3/2}$ (10^{-8} Ω cm $K^{-3/2}$)	$E_a^{(1)}$ (eV)	$E_a^{(3/2)}$ (eV)	J (meV)	T_n (K)	T_{cr} (K)
2	175	6.16	1.82	0.205	0.223	18	395	374
4	178	7.41	2.25	0.191	0.208	17	385	346
10	209	6.88	2.14	0.183	0.200	16	310	305

to the polaron potential well shown in figure 3(a) from local lattice distortions and from polarization of the surrounding spins, respectively. E_{dL} and E_{dS} are the contributions to E_d

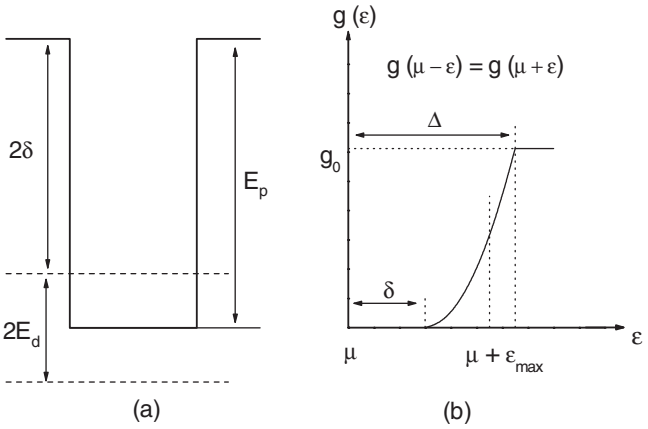

Figure 3. The polaron potential well with the depth E_p, the width of the distribution of the disorder energy $2E_d$ and the width of the rigid gap 2δ (a). The one-electron DOS $g(\varepsilon)$ with the soft gap Δ, the rigid gap δ, the maximum hopping energy ε_{max} and the DOS value outside the gap g_0 (b).

from the lattice disorder caused by random distribution of divalent ions and cation vacancies and from spin disorder, respectively. As can be seen from figure 3(a), the width of the rigid gap satisfies the equation

$$\delta = E_p/2 - E_d/2. \tag{1}$$

The one-electron DOS $g(\varepsilon)$, shown in figure 3(b), is supposed to be symmetric with respect to μ, equal to zero within the interval $(\mu - \delta, \mu + \delta)$, parabolic in the intervals $(\mu - \Delta, \mu - \delta)$, $(\mu + \delta, \mu + \Delta)$ and constant, g_0, for $\varepsilon < \mu - \Delta$ and $\varepsilon > \mu + \Delta$ [15], neglecting the small asymmetry which is important for analysis of the thermopower but does not influence the resistivity [21].

The NNH conductivity of the small lattice polarons is given by the expression [11, 20, 28, 29]

$$\rho = A_m T^m \exp[E_a^{(m)}/(kT)], \tag{2}$$

where the product $A_m T^m$ is a prefactor and $E_a^{(m)}$ is the activation energy. Let us define the energy of an intermediate state [20],

$$E_0 = e^2/(4\kappa_p)(r_p^{-1} - R_0^{-1}), \tag{3}$$

where thermal fluctuations have decreased the depth of the potential well and produced an empty potential well on a neighbouring site so that the electron can resonate between these wells. Here $\kappa_p = \kappa_\infty^{-1} - \kappa_0^{-1}$ with κ_∞ and κ_0 being the high frequency and the static dielectric constants, respectively, r_p is the small polaron radius and R_0 is the distance between the sites. If the electron can go backwards and forwards several times during the period when the two wells have the same depths, the hopping can be treated adiabatically [20, 28] yielding, for $m = 1$,

$$A_1 = \alpha k R_0/[c(1-c)e^2\omega_0] \qquad \text{and} \qquad E_a^{(1)} = E_0 - J + E_d, \tag{4}$$

where ω_0 is the optical phonon frequency and J is the electron transfer integral. Otherwise, the non-adiabatic hopping regime with $m = 3/2$,

$$A_{3/2} = \frac{\alpha' \hbar k R_0}{c(1-c)e^2 J^2}\left(\frac{4E_0 k}{\pi}\right)^{1/2} \qquad \text{and} \qquad E_a^{(3/2)} = E_0 + E_d \tag{5}$$

would set in. The parameters α and α' in equations (4) and (5), respectively, do not depend on T but may be sensitive to microscopic lattice disorder [20] and to macroscopic inhomogeneity of the material as well [30]. The condition of non-adiabatic hopping can be written in the form [20, 28, 29]

$$J^2[\pi/(4E_0kT)]^{1/2} \ll \hbar\omega_0. \tag{6}$$

Generally, the activation energy of small polaron hopping depends on T via the energy E_0 [28]. If

$$2\gamma \operatorname{csch}[\hbar\omega_0/(2kT)] \gg 1, \tag{7}$$

where γ is the (dimensionless) electron–phonon coupling constant, the temperature dependence of E_0 obeys the law [28]

$$E_0 = 2\gamma kT \tanh[\hbar\omega_0/(4kT)]. \tag{8}$$

Hence, at temperatures $T > T_D/4$ (where $T_D = \hbar\omega_0/k$ is the Debye temperature), E_0 is independent of T, so that the activation energies in the two small polaron NNH regimes defined by $m = 1$ or $3/2$ are constants differing by the value of J.

In disordered materials the probability of finding an empty nearest site with a proper energy level decreases with lowering temperature. Therefore, the conductivity is determined by competition of hoppings between the nearest sites with larger energy difference and between the sites beyond the nearest neighbours with smaller energy difference. In these conditions the hopping is possible inside an optimum energy strip $(\varepsilon_{max} - \mu, \varepsilon_{max} + \mu)$, depending on T, which leads to a deviation from the NNH conductivity law [20]. For $\varepsilon_{max} > \Delta$, the Mott VRH mechanism will set in [16, 20]; otherwise the conductivity is governed by the Shklovskii–Efros (SE) VRH mechanism [16] (this case is shown in figure 3(b)). In both cases the resistivity can be expressed in a general form,

$$\rho(T) = \rho_0(T)\exp[(T_0/T)^p], \tag{9}$$

where the prefactor $\rho_0(T)$ and the characteristic temperature T_0 depend on the VRH mechanism. If a condition $\Gamma \equiv [kT(T_0/T)^p a/(2\hbar s)]^2 \gg 1$ is satisfied, the prefactor is given by the equation

$$\rho_0(T) = AT^m \tag{10}$$

where

$$A = Ca^{11}T_0^{(7+q)p}, \tag{11}$$

s is the sound velocity and C is a constant [15]. For the SE-VRH mechanism we have $m = 9/2$ and for the Mott VRH conductivity $m = 25/4$, if the wavefunction ψ of the localized carriers has the conventional hydrogen-like form $\psi_1(r) \sim \exp(-r/a)$ corresponding to $q = 0$ in equation (11). Another form of ψ, $\psi_2(r) \sim r^{-1}\exp(-r/a)$, may set in when the fluctuating short range potential connected to the lattice disorder is important to localization [16]. In this case $q = 4$ in equation (11) and $m = 5/2$ for the SE-VRH mechanism and $m = 21/4$ for the Mott VRH conductivity in equation (10). The VRH conductivity governed by the Mott [20] and the SE [16] mechanisms is characterized by $p = 1/4$, $T_0 = T_{0M}$ or $p = 1/2$, $T_0 = T_{0SE}$, respectively, where

$$T_{0M} = \beta_M/[kg_0a^3] \qquad \text{and} \qquad T_{0SE} = \beta_{SE}e^2/(\kappa ka). \tag{12}$$

Here $\beta_M = 21$, $\beta_{SE} = 2.8$ and κ is the dielectric permittivity [16]. The presence of the rigid gap $\delta < \Delta$ modifies the SE-VRH mechanism by changing the characteristic temperature from T_{0SE} to T_0 [15] given by the equation

$$T_0 = \left(\frac{\delta}{2k\sqrt{T}} + \sqrt{\frac{\delta^2}{4k^2T} + T_{0SE}}\right)^2. \tag{13}$$

A VRH characteristic temperature may depend on T, too [15, 19]. For further consideration it is important to specify the conditions when T_0 attains a constant value. As can be seen from equations (12), T_{0SE} and T_{0M} are independent of T for constant a or g_0a^3, respectively. From equation (13) it follows that T_0 does not depend on T if, additionally, one of the following conditions is satisfied: (i) $\delta = 0$, (ii) $\delta/(2kT) \ll (T_{0SE}/T)^{1/2}$ and $\delta \sim T$ and (iii) $\delta \sim T^{1/2}$. For (ii) we have $T_0 = T_{0SE}$ because $(T_0/T)^{1/2} \approx (T_{0SE}/T)^{1/2} + \delta/(2kT)$, and if $\delta \sim T$, the second term is constant and can be included in the prefactor, while for (iii) one gets $T_0 \neq T_{0SE}$.

Equation (2) for the NNH conductivity can be reduced to the form of equation (9) by putting $A_mT^m \equiv \rho_0(T)$, $E_a^{(m)} \equiv kT_0$ and $p = 1$. Therefore, the analysis of the local activation energy $E_{loc}(T) = \mathrm{d}\ln\rho(T)/\mathrm{d}(kT)^{-1}$ [16] may be useful for identification of the hopping regime with constant T_0, as well as the temperature interval where it persists. As follows from equation (9), if T_0 is independent of T, $E_{loc}(T)$ can be expressed in the form

$$\ln[E_{loc}/(kT) + m] = \ln p + p\ln T_0 + p\ln(1/T). \tag{14}$$

Within the temperature interval corresponding to a certain hopping regime, the left-hand side of equation (14) represents a linear function of $\ln(1/T)$ for a single value of m. Then p can be found from the slope of this plot.

4. Analysis of the experimental results and discussion

4.1. NNH conductivity

As can be seen from the top panel of figure 4, at $T > T_n$ (the values of T_n are collected in table 1) the left-hand side of equation (14) can be fitted with a linear function of $\ln(1/T)$ with $m = 1$ and $3/2$, yielding values of $p = 1$ with the same fitting quality for the two values of m, as expected in the small polaron NNH regime. This confirms the NNH conductivity mechanism in LBMO above a temperature limit T_n, however, without the possibility of distinguishing between the adiabatic and non-adiabatic hopping processes. The same fitting quality in any significant temperature interval is a characteristic of the plots of $\ln(\rho/T^m)$ versus $1/T$ for both $m = 1$ and $3/2$, shown in figure 5. Such behaviour may be connected to a crossover of the adiabatic and non-adiabatic NNH regimes around T_{cr}, where $T_{cr} > T_n$ and satisfies the equation

$$A_1/A_{3/2} \approx T_{cr}^{1/2}\exp[J/(kT_{cr})], \tag{15}$$

obtained with equations (2), (4) and (5). To verify this conjecture, we fit the plots in figure 5 within the same temperature intervals, yielding the values of A_m, $E_a^{(m)}$ ($m = 1, 3/2$) and $J = E_a^{(3/2)} - E_a^{(1)}$ collected in table 1. However, it can be seen from table 1 that the values of T_{cr}, evaluated with equation (15), are definitely lower than T_n. On the other hand, because $J \ll E_a^{(m)}$, E_d is expected to be much smaller than $E_a^{(m)}$, too, and assuming that $\alpha \sim \alpha'$, we can estimate ω_0 with the expression $\omega_0 \sim (A_{3/2}/A_1)[\pi/(4E_a^{(m)}k)]^{1/2}J^2/\hbar$, following from equations (4) and (5). We obtain $\omega_0 \sim 3 \times 10^{12}$ Hz, which is much smaller than $\omega_0 \approx kT_D/\hbar \approx 5 \times 10^{13}$ Hz for $T_D \approx 400$ K found from the low temperature specific heat of $La_{0.67}Ba_{0.33}MnO_3$ [31]. In addition, above T_n the right-hand side of the inequality (6), $\hbar\omega_0 \approx kT_D \approx 30$ meV considerably exceeds the left-hand side $\sim J^2[\pi/(4E_a^{(m)}kT)]^{1/2} <$ 4 meV. These relations suggest that the NNH conductivity regime in LBMO is non-adiabatic, assuming that at $T > T_n$ the spin dependent effects are small.

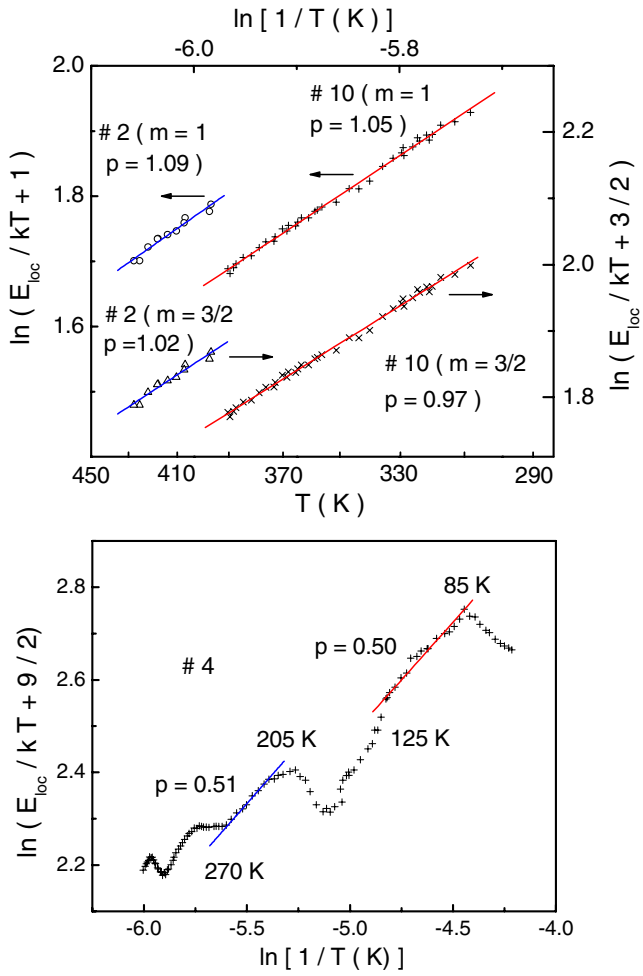

Figure 4. The plots of $\ln(E_{\rm loc}/kT{+}1)$ versus $\ln(1/T)$, $\ln(E_{\rm loc}/kT\,+\,3/2)$ versus $\ln(1/T)$ (upper panel) and $\ln(E_{\rm loc}/kT\,+\,9/2)$ versus $\ln(1/T)$ (lower panel). The solid lines are the linear fits to the experimental data.

4.2. VRH conductivity

The plots in figure 5 deviate from linearity below T_n, which is well above $T_{\rm C}$ (table 1). Because $T_{\rm C} > T_{\rm D}/4$, this deviation cannot be connected to the temperature dependence of the NNH activation energy due to equation (8), but should be ascribed to a transition to the VRH conductivity. The analysis of the local activation energy with equation (14) reveals two intervals of linearity of the plots $\ln(E_{\rm loc}/kT + m)$ versus $\ln(1/T)$, above and below $T_{\rm C}$, yielding $m = 9/2$ and $p = 1/2$ on each interval, with no evidence for any other possible pairs of m and p in the VRH conductivity regime (figure 4, bottom panel). Such behaviour of the resistivity corresponds to the SE-like VRH conductivity mechanism, with at least one type of gap, Δ, of $g(\varepsilon)$ (section 3). The plots of $\ln(\rho/T^{9/2})$ versus $T^{-1/2}$ in figure 6 support this conclusion, containing the intervals of the linear behaviour both above $T_{\rm C}$ (marked by the open triangles in the upper panel) and below it. From the linear parts of the plots in figures 4 and 6 we obtain the values of the VRH onset temperature, $T_{\rm v}$, and those of A and T_0 in equations (9) and (10) for $T > T_{\rm C}$ (denoted as $A_{\rm ht}$ and $T_{0\rm ht}$) and $T < T_{\rm C}$ (denoted as $A_{\rm lt}$ and $T_{0\rm lt}$), as collected in table 2. The width of the Coulomb gap, shown in table 2, is evaluated using the expression $\Delta \approx k(T_{\rm v}T_{0\rm ht})^{1/2}$ [15]. With the equation $\Delta \approx U$, where $U \approx e^2/(\kappa R)$

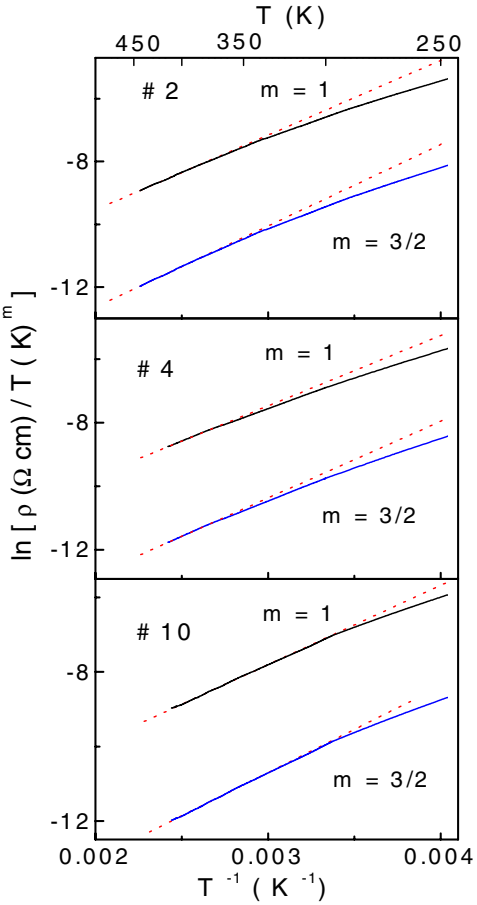

Figure 5. The dependences of $\ln(\rho/T^m)$ on T^{-1} for $m = 1$ and $3/2$. The dotted lines are linear fits.

Table 2. The values of the high temperature, $A_{\rm ht}$, and the low temperature, $A_{\rm lt}$, prefactor coefficients of the VRH conductivity, the high temperature, $T_{0\rm ht}$, and the low temperature, $T_{0\rm lt}$, characteristic temperatures of the VRH conductivity, and the width of the Coulomb gap, Δ.

Sample Nos	$A_{\rm ht}$ (10^{-20} Ω cm K$^{-9/2}$)	$A_{\rm lt}$ (10^{-20} Ω cm K$^{-9/2}$)	$T_{0\rm ht}$ (10^4 K)	$T_{0\rm lt}$ (10^4 K)	Δ (eV)
2	2.81	12.5	10.3	8.6	0.44
4	1.73	7.14	10.4	8.8	0.46
8	3.48	2.94	9.5	7.1	0.44
10	3.35	4.48	9.5	6.9	0.44

is the Coulomb interaction energy, $R = 2(4\pi N_0 c/3)^{-1/3}$ is the mean distance between the holes, $N_0 = 1.3 \times 10^{22}$ cm^{-3} is the concentration of the Mn ions and $c \approx 0.16$–0.17 is the relative concentration of the holes in the samples (a slow variation of c is connected to a strong influence of the cation vacancies to the hole doping of LBMO between $x = 0.02$ and 0.10 [9]), we obtain $\kappa \approx 3.2$ for No 4 and $\kappa \approx 3.4$ for No 2, No 8 and No 10.

The existence of temperature intervals where T_0 is constant, as evident from figures 4 and 6, suggests that one of the cases, mentioned in the comments on equation (13) of section 3, takes place. To find which case is realized, we analyse the temperature dependence of the

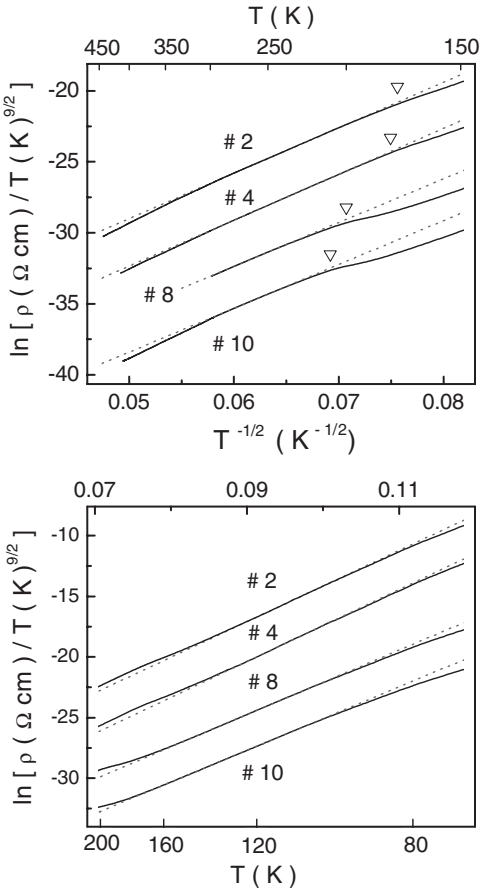

Figure 6. The plots of $\ln(\rho/T^{9/2})$ versus $T^{-1/2}$ above T_C (upper panel) and below T_C (lower panel). The dotted lines are linear fits. For convenience the curves for No 4, No 8 and No 10 are shifted along the Y-axes by -3, -6 and -9 units. The open triangles mark T_C.

resistivity in the magnetic field. The localization radius of small polarons in the PM phase was predicted to vary in the field according to the law [32]

$$a(B) = a(0)(1 + b_1 B^2), \tag{16}$$

where $b_1 \sim \chi(T)$. If $b_1 B^2 \ll 1$, it follows from equations (12), (13) and (16) that

$$T_0(B) = T_0(0)(1 - b_2 B^2), \tag{17}$$

where $b_2 = b_1 T_{0SE}(0)\{T_0(0) - [T_0(0)/T]^{1/2}\delta/(2k)\}^{-1}$ until δ is independent of B. This gives

$$\delta(T) = 2\frac{b_1/b_2 - 1}{2b_1/b_2 - 1} k\sqrt{T_0(0)T}. \tag{18}$$

Near T_v well above T_C, the temperature dependence of χ can be neglected (figure 1, inset). Therefore, at temperatures in the vicinity to T_v the dependences of T_0 and A on B can be found from linear fits of the plots of $\ln(\rho/T^{9/2})$ versus $T^{-1/2}$ in the field. The dependence of $a(B)/a(0)$ can be evaluated with equation (11). From the linear fits of the plots of $a(B)/a(0)$ versus B^2 and $T_0(B)/T_0(0)$ shown in figure 7 we obtain $b_1 = (1.6 \pm 0.2) \times 10^{-3}$ T^{-2}, $b_2 \approx (1.3 \pm 0.2) \times 10^{-3}$ T^{-2} and $b_1 = (6.0 \pm 0.3) \times 10^{-3}$ T^{-2}, $b_2 = (4.5 \pm 0.2) \times 10^{-3}$ T^{-2} for No 4 and No 10, respectively. The difference between b_1 and b_2 exceeds the error, which means due to equation (18) the existence of a non-zero rigid gap, depending on T close to the

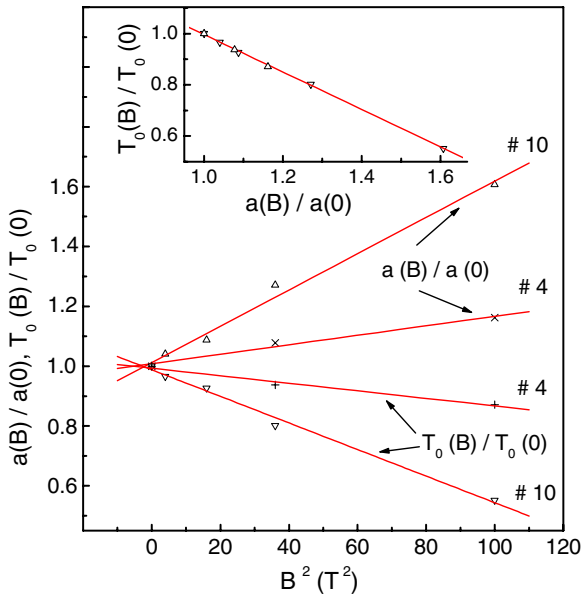

Figure 7. The dependences of $a(B)/a(0)$ and $T_0(B)/T_0(0)$ on B^2. The lines are linear fits. Inset: the dependence of $T_0(B)/T_0(0)$ on $a(B)/a(0)$ for No 4 (Δ) and No 10 (∇). The line is a linear fit of the data.

function $\delta(T) \approx \delta_v(T/T_v)^{1/2}$, where $\delta_v \equiv \delta(T_v) \approx 0.14$ eV and 0.18 eV for No 4 and No 10, respectively, are evaluated with equation (18) at $T = T_v$ and $T_0(0) = T_{0ht}$ (table 2). Using the values of δ_v, T_{0ht} (table 2) and κ found above, we get with equations (12) and (13) in the temperature interval corresponding to $T_0 = T_{0ht}$ and $\delta(T) \approx \delta_v(T/T_v)^{1/2}$ the localization radii $a_{ht} \approx 2.0$ Å for No 4 and $a_{ht} \approx 2.4$ Å for No 10.

To find the behaviour of a, T_0 and δ in an extended temperature interval, we present equation (9) with equations (10) and (11) in the form

$$\ln\left[\frac{\rho(T)}{\rho(T_v)}\left(\frac{T_v}{T}\right)^{9/2}\right] = 11\ln\left(\frac{a}{a_{ht}}\right) + \frac{7}{2}\ln\left(\frac{T_0}{T_{0ht}}\right) + \left(\frac{T_0}{T}\right)^{1/2} - \left(\frac{T_{0ht}}{T_v}\right)^{1/2}, \tag{19}$$

containing two parameters, T_0/T_{0ht} and a/a_{ht}, the relation of which can be obtained by excluding B from the magnetic field dependences of $T_0(B)/T_0(0)$ and $a(B)/a(0)$ in figure 7. As is evident from the inset to figure 7, this relation is close to linear. Hence, equation (19) can be solved numerically with respect to a/a_{ht} by excluding T_0/T_{0ht} with a linear function obtained by fitting the plots of $T_0(B)/T_0(0)$ versus $a(B)/a(0)$ in the inset to figure 7. As can be seen from the upper panel of figure 8, the functions $a(T)/a_{ht}$ and $T_0(T)/T_{0ht}$ obtained as described above exhibit intervals of constancy above and below T_C, over the same intervals of the constant slopes in figure 4 (lower panel) and figure 6, separated by the intervals of steep variation around T_C. The ratio of the values of T_0 on the intervals of constancy coincides with T_{0ht}/T_{0lt}. In addition, $a(T)/a_{ht}$ increases and $T_0(T)/T_{0ht}$ decreases with decreasing temperature below $T_q \sim 100$ K. Finally, the dependence of $\delta(T)$ is evaluated with equation (13) and shown in figure 9 for No 4 and in figure 10 for No 10. It can be seen that $\delta(T) \approx \delta_v(T/T_v)^{1/2}$ and $\delta(T) \approx \delta'_v(T/T_v)^{1/2}$, where $\delta'_v \approx 0.132$ eV for No 4 and 0.155 eV for No 10 (dotted lines in figures 9 and 10) in the intervals of constancy of $a(T)$, $T_0(T)$ below and above T_C, respectively. Additionally, $\delta(T)$ exhibits an inflection around T_C and deviates from the square-root dependence at $T < T_q$.

As mentioned in the introduction, the rigid gap originates in the manganite perovskites from the small polaron nature of the charge carriers. Well below T_C, due to a strong FM interaction between the Mn ions, the contribution to E_p from polarization of the Mn ion spins may be expected to be small, and $E_p \approx E_{pL}$. Hence, taking into account the relation

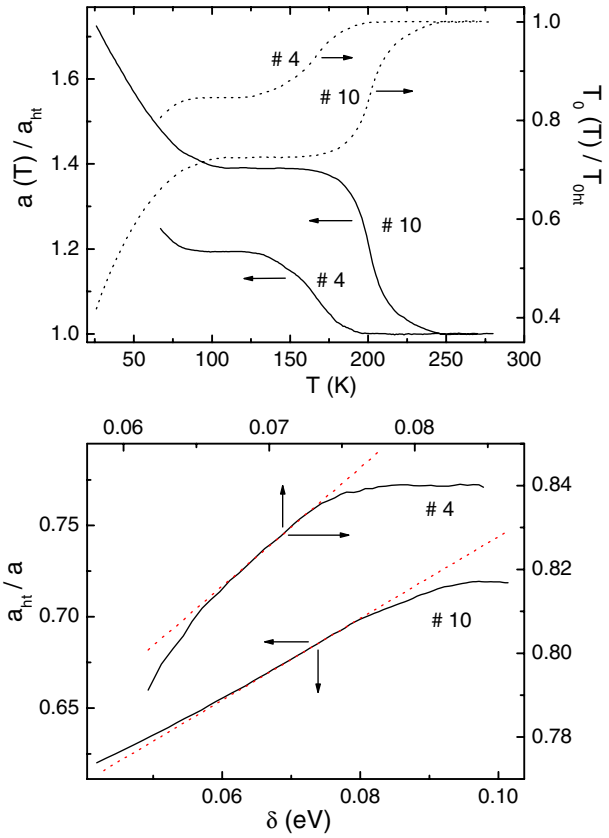

Figure 8. The dependences of $a(T)/a_{\rm ht}$ and $T_0(T)/T_{0\rm ht}$ on temperature (upper panel). The plots of $a_{\rm ht}/a$ versus δ (lower panel). The dotted lines are the linear fits.

$E_0 \approx E_{\rm pL}/2$ [20, 28] and equation (1), we obtain

$$\delta(T) \approx E_0(T) - E_{\rm d}/2, \tag{20}$$

up to $T \sim T_q$. To use equation (8), we must specify its lower limit of applicability given by the condition in equation (7). Below T_q it can be rewritten as $T > T_t$, where $T_t \approx T_{\rm D}/[2\ln(4\gamma)]$. The electron–phonon interaction is strong enough in weakly doped manganite perovskites to cause the persistence of the electron localization and the activation behaviour of the resistivity down to $T \ll T_{\rm C}$. Then, putting e.g. $\gamma \sim 10$, with $T_{\rm D} \approx 400$ K [31], we obtain $T_t \sim 50$ K. The interval of applicability of the expression

$$\delta(T) \approx 2\gamma kT \tanh[\hbar\omega_0/(4kT)] - E_{\rm d}/2, \tag{21}$$

following from equation (8) and the equation for $\delta(T)$ above, can be found more accurately, along with an estimate of γ, by using the linear approximation $\tanh[\hbar\omega_0/(4kT)] \approx \tanh[T_{\rm D}/(4T)] = \alpha_0 - \alpha_1 T$ with $\alpha_0 = 1.179$ and $\alpha_1 = 4.150 \times 10^{-4}$ K^{-1}, valid between $T = 50$ and 100 K. Then, neglecting a weak temperature dependence of $E_{\rm d}$ (which could stem only from the spin disorder, exhibiting no strong dependence on T well above $T_{\rm C}$), and differentiating equation (20) over T, we have $\delta'(T) \approx 2\alpha_0\gamma k - 4\alpha_1\gamma kT$, where $\delta'(T) \equiv {\rm d}\delta(T)/{\rm d}T$. The linear approximation of the functions $\delta'(T)$ in the insets to figures 9 and 10 yields $T_t \approx 55$ K for No 10, $T_t < 68$ K for No 4 and $\gamma \sim 7$–9 for both samples. The fit of $\delta(T)$ with equation (20) (the dashed line in figures 9 and 10) within the interval of linearity of $\delta'(T)$ by the variation of γ between 7 and 9 and ω_0 around $kT_{\rm D}/\hbar = 5.2 \times 10^{13}$ Hz gives more

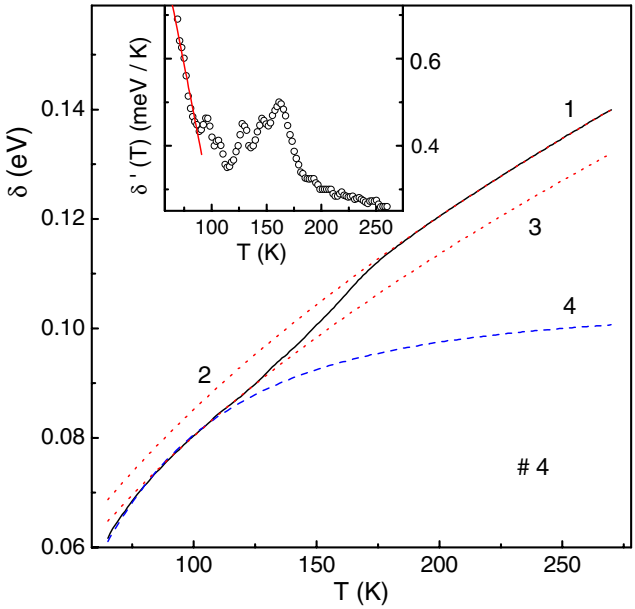

Figure 9. Temperature dependence of the width of the rigid gap (line 1), the approximating functions $\delta_v(T/T_v)^{1/2}$ (line 2) and $\delta'_v(T/T_v)^{1/2}$ (line 3) and the function evaluated with equation (21) as described in the text (line 4) for No 4. Inset: temperature dependence of the derivative $\delta'(T) = \mathrm{d}\delta(T)/\mathrm{d}T$ for No 4. The line is the linear fit.

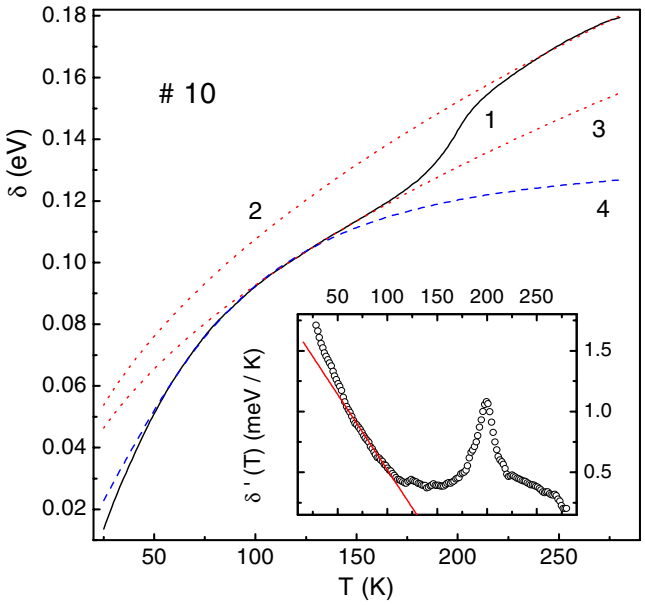

Figure 10. Temperature dependence of the width of the rigid gap (line 1), the approximating functions $\delta_v(T/T_v)^{1/2}$ (line 2) and $\delta'_v(T/T_v)^{1/2}$ (line 3) and the function evaluated with equation (21) as described in the text (line 4) for No 10. Inset: temperature dependence of the derivative $\delta'(T) = \mathrm{d}\delta(T)/\mathrm{d}T$ for No 10. The line is the linear fit.

accurate values of $\gamma \approx 8.5$ and $\omega_0 \approx 4.5 \times 10^{13}$ Hz for No 4, $\gamma \approx 7.1$ and $\omega_0 \approx 6.1 \times 10^{13}$ Hz for No 10, and $E_d \approx 0.043$ eV and 0.015 eV for No 4 and No 10, respectively.

To analyse the temperature dependence of the localization radius below T_q, with equation (3) at $r_p = a$ and equation (20), we obtain

$$\frac{1}{a(T)} = \frac{1}{R_0} + \frac{4\kappa_p}{e^2}\left[\delta(T) + \frac{E_d}{2}\right], \tag{22}$$

suggesting a linear dependence of a^{-1} on δ between T_q and T_t. As can be seen from the bottom panel of figure 8, the plot of a_{ht}/a versus δ for No 10 contains a linear part, corresponding approximately to the interval (T_t, T_q), whereas for No 4 the deviation from linearity takes place at $T > T_t$. This is connected with a limited applicability of the linear dependence of T_0/T_{0ht} on a/a_{ht}, used above, which breaks for No 10 below T_t and for No 4 already above T_t. From the linear part of the plots in the bottom panel of figure 8, with $R_0 = 2(4\pi N_0/3)^{-1/3} \approx 5.3$ Å, we obtain $\kappa_p \approx 5.3$ and $E_d \approx 0.050$ eV for No 4, and $\kappa_p \approx 3.3$ and $E_d \approx 0.017$ eV for No 10.

4.3. Discussion

The values of the localization radius, obtained above for the samples No 4 and No 10, are smaller than the mean distance between the Mn sites, $R_0 \approx 5.3$ Å, satisfying the requirement for small polaron formation [20]. It can be shown also that the condition of $\Gamma \gg 1$ is satisfied over the whole temperature interval investigated. The values of κ_p are comparable with those evaluated with the values of κ_0 and κ_∞ given in the limits of $\kappa_0 = 16$–21 and $\kappa_\infty = 3.4$–3.9 [33], yielding $\kappa_p \approx 4.1$–5.2. Values of $\kappa \approx 3.4$ and 3.5, close to those in LBMO (this work), have been found earlier for $La_{0.7}Ca_{0.3}Mn_{1-y}Fe_yO_3$ [15] and for $LaMnO_{3+\eta}$ [19]. They are much smaller than κ_0, whereas for the doped semiconductors $\kappa = \kappa_0$ [18]. On the other hand, the values of κ are much closer to κ_p, than to κ_0. As mentioned in the introduction, in the manganite perovskites the concentration of the charge carriers (equal to the concentration of holes) is much higher than in doped semiconductors. In addition, the carriers in the manganite perovskites are small polarons, whereas in conventional (non-magnetic) semiconductors the polaron effects are negligible [16]. High concentration of the polarons leads to an average mutual distance comparable with the lattice parameters. On the other hand, the main contribution to Δ is connected to the interaction between the nearest carriers. However, the field around the polaron is characterized not by κ_0, but by κ_p [20]. Therefore, the electrostatic interaction between the polarons at the distance R deviates from the conventional Coulomb law and is described by the expression $U \approx e^2/(\kappa_p R)$. However, in the case of small polarons the situation is even more complicated, because then the dielectric permittivity generally depends not only on the frequency but also on the wavevector [28], which does not permit macroscopic averaging even at a low polaron concentration [28]. Therefore, utilization of macroscopic parameters such as κ_0 and κ_∞ has only a limited applicability, leading in particular to different values of κ_p for the samples No 4 and No 10.

The large value of the coupling constant γ indicates a strong electron–phonon interaction, supporting the leading role of local Jahn–Teller distortions [10] in the localization of the charge carriers and formation of the small polaron state. The values of $\gamma = 7.1$–8.5 found for LBMO in this work are comparable with those, up to $\gamma \approx 9.3$, for $LaMnO_{3+\eta}$ [34]. The values of E_d, obtained from analysis of a, are close to those determined from the temperature dependence of $\delta(T)$, in the same intervals of low T between T_t and T_q. It can be seen also that the value of E_d for No 4 exceeds that for No 10. This correlates well with the enhanced lattice disorder in No 4, as may be concluded from the dependence of T_C on x, and the role of the cation vacancies in the hole doping [9]. On the high temperature part of the temperature interval investigated, E_d is close to $(2/3)\ (E_a^{(3/2)} - \delta_v) \approx 0.045$ eV for No 4 and 0.013 eV for No 10,

which suggests that the spin dependent contributions to E_p and E_d are small in the limits of high and low temperatures. At high temperatures, corresponding to the NNH conductivity, the spin polarization of the Mn ions is suppressed by rapid spin relaxation processes, whereas at temperatures well below T_C it is hindered by the strong FM DE interaction. The phase separation effect responsible for the spin disorder in the manganite perovskites is also most pronounced as $T \to T_C$ [9, 35]. This explains the similarity of E_d in the limits of high and low temperatures due to the smallness of spin dependent contributions to E_p and E_d. However, this may not be so around T_C, which may lead to inflection of $\delta(T)$. On the other hand, the inflection and the rapid variation of $\delta(T)$ near T_C cannot be explained just by the spin effects, leading to a too large contribution of the spin polarization on the NNH conductivity interval, $E_{pS} \approx 2\delta_v - \gamma\hbar\omega_0 + E_d \approx 0.08$ eV and 0.09 eV, comparable with the high temperature lattice contribution $E_{pL} \approx \gamma\hbar\omega_0 \approx 0.25$ eV and 0.28 eV for No 4 and No 10, respectively. Therefore, the lattice contribution to E_p should also have a rapid variation near T_C, which can explain the steep increase of a around T_C with lowering T (top panel of figure 8). In turn, the square-root dependence of $\delta(T)$ is evidently not connected to the lattice polarization and disorder, deviating from the dependence given by equation (21), and is attributable to the spin effects. It persists down to T_q, excluding an interval around T_C, and may be due to both the spin polarization and the spin disorder, which cannot be distinguished in our study, or some interplay between them. It is possible to suppose that the spin dependent effects may be sensitive to the mean hopping length, $R_h \sim T^{-1/2}$ on the SE-like VRH interval, and $R_h \approx R_0$ on the NNH interval [16]. Indeed, if the hopping electron were responsible also for the spin correlations between the Mn ions, the correlation radius would be determined by the mean hopping length. On the other hand, since R_h increases with lowering T, the hopping electron becomes more sensitive to spin disorder due to the phase separation, having a nanometre scale [7, 8]. Therefore, the square-root dependence of δ may be connected to a transition to the VRH regime and vanishes in the NNH conductivity interval, providing a constant NNH activation energy.

5. Conclusions

We have investigated the resistivity of ceramic low doped $La_{1-x}Ba_xMnO_3$ with $x \leqslant 0.1$ within the broad temperature interval between $T = 25$ and 450 K, both above and below the PM–FM transition temperature. At high temperatures ρ is determined by the small polaron NNH conductivity mechanism, satisfying the conditions of non-adiabatic hopping. With lowering temperature the SE-like VRH conductivity sets in, corresponding to the Coulomb gap superimposed by the rigid gap in the one-electron density of the localized states. The width of the rigid gap depends on T similarly to the square-root law, deviating from this behaviour in the vicinity to T_C and with lowering temperature well below T_C. At low temperatures, $\delta(T)$ is determined by formation of small lattice polarons under the conditions of strong electron–phonon interaction and lattice disorder. The localization radius exhibits two intervals of constancy, the same as those of the dependence of $\delta(T) \sim T^{-1/2}$, characterized by different values of a, and an interval of steep variation with T around T_C. With lowering temperature $a(T)$ increases in a way characteristic of small polarons. Also the values of a satisfy the condition for small polaron formation.

Generally, the one-electron model gives a satisfactory description of the hopping mechanisms and their variation in the different temperature intervals with reasonable numerical values of a and $\delta < \Delta$. However, the model provides only an approximative description of the electrostatic interaction of the polarons, which is renormalized strongly by multi-electron effects (κ_0 is changed to κ_p in the interaction energy law) and has, additionally, a limited applicability with respect to the macroscopic dielectric permittivity parameters (κ_0 and κ_∞).

Acknowledgments

This work was supported by the Wihuri Foundation, Finland, and by INTAS (Project No INTAS 00-00728).

References

[1] Von Helmolt R, Wecker J, Holzapfel B, Schulz L and Sammer K 1993 *Phys. Rev. Lett.* **71** 2331
[2] Coey J M D, Viret M and von Molnar S 1999 *Adv. Phys.* **48** 167
[3] de Gennes P-G 1960 *Phys. Rev.* **118** 141
[4] de Almeida J R L 1999 *J. Phys.: Condens. Matter* **11** L223
[5] Laiho R, Lähderanta E, Salminen J, Lisunov K G and Zakhvalinskii V S 2001 *Phys. Rev.* B **63** 094405
[6] Laiho R, Lisunov K G, Lähderanta E, Petrenko P A, Salminen J, Stamov V N and Zakhvalinskii V S 2000 *J. Phys.: Condens. Matter* **12** 5751
[7] Chechersky V, Nath A, Isaac I, Franck J P, Ghosh K, Ju H and Greene R L 1999 *Phys. Rev.* B **59** 497
[8] Hennion M, Moussa F, Biotteau G, Rodriguez-Carvajal J, Piusard L and Revcolevschi A 1998 *Phys. Rev. Lett.* **81** 1957
[9] Laiho R, Lisunov K G, Lähderanta E, Zakhvalinskii V S, Kozhevnikov V L, Leonidov I A, Mitberg E B and Patrakeev M V 2005 *J. Magn. Magn. Mater.* at press
[10] Millis A J, Littlewood P B and Shraiman B I 1995 *Phys. Rev. Lett.* **74** 5144
[11] Jaime M, Salamon M B, Rubinstein M, Treece R E, Horwitz J S and Chrisei D B 1996 *Phys. Rev.* B **54** 11914
[12] Ramirez A P 1997 *J. Phys.: Condens. Matter* **9** 8171
[13] Snyder G J, Hiskes R, DiCarolis S, Beasley M R and Geballe T H 1996 *Phys. Rev.* B **53** 14434
[14] Worledge D C, Snyder G J, Beasley M R and Geballe T H 1996 *J. Appl. Phys.* **80** 5158
[15] Laiho R, Lisunov K G, Lähderanta E, Petrenko P A, Salminen J, Shakhov M A, Safontchik M O, Stamov V S, Shubnikov M V and Zakhvalinskii V S 2002 *J. Phys.: Condens. Matter* **14** 8043
[16] Shklovskii B I and Efros A L 1984 *Electronic Properties of Doped Semiconductors* (Berlin: Springer)
[17] Biswas A, Elizabeth S, Raychaudhuri A K and Bhat H L 1999 *Phys. Rev.* B **59** 5368
[18] Castner T G 1991 *Hopping Transport in Solids* ed M Pollak and B Shklovskii (Amsterdam: Elsevier) p 3
[19] Laiho R, Lisunov K G, Lähderanta E, Stamov V N, Zakhvalinskii V S, Colomban Ph, Petrenko P A and Stepanov Yu P 2005 *J. Phys.: Condens. Matter* **17** 105
[20] Mott N F and Davies E A 1979 *Electron Processes in Non-Crystalline Materials* (Oxford: Clarendon)
Mott N F 1990 *Metal–Insulator Transitions* (London: Taylor and Francis)
[21] Laiho R, Lisunov K G, Lähderanta E, Stamov V N, Zakhvalinskii V S, Kurbakov A I and Sokolov A E 2004 *J. Phys.: Condens. Matter* **16** 881
[22] Yuan S L, Jiang Y, Li G, Yang Y P, Zeng X Y, Tang P and Huang Z 2000 *Phys. Rev.* B **61** 3211
[23] Mandal P 2000 *Phys. Rev.* B **61** 14 675
[24] Mandal P and Gosh B 2003 *Phys. Rev.* B **68** 014422
[25] Cherepanov V A, Filonova E A, Voronin V I and Berger I F 2000 *J. Solid State Chem.* **153** 205
[26] Laiho R, Lisunov K G, Lähderanta E, Salminen J and Zakhvalinskii V S 2002 *J. Magn. Magn. Mater.* **250** 267
[27] Laiho R, Lisunov K G, Lähderanta E, Petrenko P A, Salminen J, Stamov V N, Stepanov Yu P and Zakhvalinskii V S 2003 *J. Phys. Chem. Solids* **64** 2313
[28] Appel J 1968 *Solid State Physics* vol 21, ed F Seitz, D Turnbull and H Ehrenreich (New York: Academic) p 193
[29] Raffaelle R, Anderson H U, Sparlin D M and Parris P E 1991 *Phys. Rev.* B **43** 7991
[30] Gupta A, Gong G Q, Xiao G, Duncombe P R, Lecoeur P, Trouilloud P, Wang Y Y, Dravid V P and Sun J Z 1996 *Phys. Rev.* B **54** R15629
[31] Hamilton J J, Keatley E L, Ju H L, Raychaudhuri A K, Smolyaninova V N and Greene R L 1996 *Phys. Rev.* B **54** 14926
[32] Varma C M 1996 *Phys. Rev.* B **54** 7328
[33] Alexandrov A S and Bratkovsky A M 2000 *J. Appl. Phys.* **87** 5016
[34] Pal S, Banerjee A, Rosenberg E and Chaudhuri B K 2001 *J. Appl. Phys.* **87** 4955
[35] Yunoki S, Moreo A and Dagotto E 1998 *Phys. Rev. Lett.* **81** 5612
Okamoto S, Ishihara S and Makaeva S 2000 *Phys. Rev.* B **61** 451